Solution Structure of a Sweet Protein Single-Chain Monellin Determined by Nuclear Magnetic Resonance and Dynamical Simulated Annealing Calculations[†,‡]

Seok-Yong Lee,[§,||] Jung-Hoon Lee,[§] Ho-Jin Chang,[⊥] Joong Myung Cho,[⊥] Jin-Won Jung,[§] and Weontae Lee*[,§]

Department of Biochemistry, College of Science, Yonsei University, Seoul 120-740, Korea, and Biotech Research Institute, LG Chemical, Research Park, P.O. Box 61, Yu-Sung, Science Town, Taejon 305-380, Korea

Received September 22, 1998; Revised Manuscript Received November 30, 1998

ABSTRACT: Single-chain monellin (SCM), which is an engineered 94-residue polypeptide, has proven to be as sweet as native two-chain monellin. SCM is more stable than the native monellin for both heat and acidic environments. Data from gel filtration HPLC and NMR indicate that the SCM exists as a monomer in aqueous solution. The solution structure of SCM has been determined by nuclear magnetic resonance (NMR) spectroscopy and dynamical simulated annealing calculations. A stable α-helix spanning residues Phe11−Ile26 and an antiparallel β-sheet formed by residues 2−5, 36−38, 41−47, 54−64, 69−75, and 83−88 have been identified. The sheet was well defined by backbone−backbone NOEs, and the corresponding β-strands were further confirmed by hydrogen bond networks based on amide hydrogen exchange data. Strands β2 and β3 are connected by a small bulge comprising residues Ile38−Cys41. A total of 993 distance and 56 dihedral angle restraints were used for simulated annealing calculations. The final simulated annealing structures ($\langle SA \rangle_k$) converged well with a root-mean-square deviation (rmsd) between backbone atoms of 0.49 Å for secondary structural regions and 0.70 Å for backbone atoms excluding two loop regions. The average restraint energy-minimized (REM) structure exhibited root-mean-square deviations of 1.19 Å for backbone atoms and 0.85 Å for backbone atoms excluding two loop regions with respect to 20 $\langle SA \rangle_k$ structures. The solution structure of SCM revealed that the long α-helix was folded into the concave side of a six-stranded antiparallel β-sheet. The side chains of Tyr63 and Asp66 which are common to all sweet peptides showed an opposite orientation relative to H1 helix, and they were all solvent-exposed. Residues at the proposed dimeric interface in the X-ray structure were observed to be mostly solvent-exposed and demonstrated high degrees of flexibility.

A sweet protein monellin was originally isolated from the berries of the West African plant *Dioscoreophyllum cumminsii* (*1*, *2*). The studies for molecular interactions of different sweeteners with receptor as well as a receptor binding model have been proposed previously (*3*−*9*). A sweet protein, monellin, consists of two separate polypeptide chains which are an A chain of 45 residues and a B chain of 50 residues. Three other sweet proteins which are thaumatin, pentadin, and mabinlin have also been discovered (*10*−*14*). It has been reported that a curculin protein which was extracted from the fruits of *Curculigo latifolia* demonstrated not only sweet taste but also taste-modifying activity (*15*). Monellin is approximately 70 000 times sweeter than sucrose and 300 times sweeter than the dipeptide sweetener aspartame (*16*, *17*). The crystal structure of native two-chain monellin has been determined at 2.75 Å resolution, showing the two chains are packed closely by both hydrogen bonds and hydrophobic interactions (*18*). Native monellin has a β-sheet comprised of five antiparallel strands and a single 17-residue long α-helix from the B chain. The crystal structure showed that the amino terminus of the A chain is connected to the carboxyl terminus of the B chain through intermolecular hydrogen bond networks. It has been observed that the long α-helix is folded into the concave side of a twisted antiparallel β-sheet (*18*).

Recently, the alcohol-denatured state of native monellin was characterized and displayed a β-sheet to α-helix structural reorganization of the A chain in 50% ethanol and 50% trifluoroethanol (TFE) solution (*19*). In addition, the conformation and dynamics of both native and mutated nonsweet analogue monellin have been studied by two-dimensional (2D) nuclear magnetic resonance spectroscopy. It has been reported that the three-dimensional structures of native monellin and two thiol proteinase inhibitors, cystatin and stefin B, are very similar (*20*). Therefore, on the basis of those structural homologies, it has been suggested that

[†] This study was supported by the Yonsei University Research Fund of 1997 (W.L.).

[‡] The atomic coordinates for 20 simulated annealing structures and the energy-minimized average structure have been deposited (accession code 1mnl) with the Protein Data Bank, Brookhaven National Laboratories, P.O. Box 5000, Upton, Long Island, NY 11973-5000.

* To whom correspondence should be addressed: Department of Biochemistry, College of Science, Yonsei University, Seodaemoon-Gu, Shinchon-Dong, Seoul 120-740, Korea. Telephone: 82-2-361-2706. Fax: 82-2-362-9897. E-mail: wlee@nestis.yonsei.ac.kr.

[§] Yonsei University.

[||] Present address: Graduate Group in Biophysics, University of California at Berkeley, Berkeley, CA 94720.

[⊥] LG Chemical.

[1] Abbreviations: SCM, single-chain monellin; NMR, nuclear magnetic resonance; 1D, one-dimensional; 2D, two-dimensional; NOESY, nuclear Overhauser effect spectroscopy; TOCSY, total correlated spectroscopy; DQF-COSY, double-quantum-filtered correlated spectroscopy; HSQC, heteronuclear single-quantum coherence; SA, simulated annealing; REM, restraint energy-minimized.

10.1021/bi9822731 CCC: $18.00
Published on Web 02/04/1999

monellin protein may have some other biological role beside its sweetness.

On the basis of the crystallographic structure of native two-chain monellin, single-chain monellin (SCM)[1] was recently constructed by fusing the two chains to maintain the topology of monellin (*21*). SCM, an engineered 94-residue polypeptide, has proven to be as sweet as native monellin. In addition, SCM is more stable than the native two-chain monellin for both heat and acidic environments (*21*). The crystal structure of SCM has been reported to be a dimer conformation in the asymmetric unit. The structure revealed that the major driving forces for dimeric contacts are predominantly hydrophobic interactions involved in side chains of Trp3, Ile5, Pro40, Met42, and Tyr61 as well as proline residues in the C terminus (*22*). Recently, a two-dimensional ^{1}H NMR study has also been performed for recombinant SCM and provided strong evidence for the monomer conformation in the solution state (*23*). Thereby, it is very likely that SCM could exist as a monomer in aqueous solution. However, it was not possible to compare the solution structure with the X-ray crystal structure unambiguously because the NMR sample used by Tomic et al. (*23*) exhibited a mixture of two distinct amino terminal sequences. Since there is no information about the receptor binding structure of SCM, the solution structure would provide a structural background about sweet taste as well as structural stability in solution. Here, we present the high-resolution solution structure of SCM determined by multidimensional NMR spectroscopy combined with distance geometry and dynamical simulated annealing calculations.

EXPERIMENTAL PROCEDURES

Expression and Purification of SCM. *Saccharomyces cerevisiae* AB110 was used for expression of the recombinant monellin. Transformed yeast cells were propagated in yeast nitrogen base containing 5% glucose and 0.5% ammonium sulfate at 30 °C for 2 h and grown in M9 media containing 2% glucose and 0.1% ammonium sulfate at 30 °C for 48 h. For uniformly ^{15}N-labeled monellin, the cells were grown on minimal medium containing ^{15}N-labeled ammonium sulfate as the sole source of the nitrogen. The cells were harvested by centrifugation at 3500 rpm for 25 min. Cells were stored at −80 °C and used for purification procedures. Cell pastes were disrupted by a bead beator in 25 mM sodium phosphate, 5 mM EDTA, 150 mM NaCl, and 1 mM PMSF at pH 7.0. The cell lysates were centrifuged to collect supernatants at 12 000 rpm for 215 min. After pH adjustment and centrifugation, the supernatants were diluted with 10 mM sodium phosphate and loaded onto a CM-Sepharose column. The bound monellin was eluted with a salt gradient. The collected protein solutions were dialyzed and dried with a freeze-dryer for NMR experiments.

NMR Spectroscopy. The protein samples for NMR measurements were dissolved in either 90% H_2O/10% D_2O or 99.9% D_2O solutions in 50 mM sodium phosphate at pH 7.0. The final protein concentration was 1.5−2.0 mM in 0.5 mL of solution. All NMR experiments were performed on a Bruker DMX-600 spectrometer in quadrature detection mode equipped with a triple-resonance probe with an actively shielded pulsed-field gradient (PFG) coil. Most of the experiments were performed at either 25 or 30 °C, and the temperature was calibrated using a methanol standard (*24*). Pulsed-field gradient techniques with a WATERGATE sequence (*25*) were used for all H_2O experiments, resulting in a good suppression of the solvent signal. Mixing times of 50−200 ms were used in collecting NOE spectra (*26*, *27*). Total correlation spectroscopy (TOCSY) (*28*) data were also recorded in H_2O solution with a mixing time of 78 ms using MLEV17 spin lock pulses. Double-quantum-filtered (DQF) COSY (*29*) spectra were collected in H_2O solution to obtain vicinal coupling constant information. All data were recorded in the phase sensitive mode using the time-proportional phase incrementation (TPPI) method (*30*) with 2048 data points in the t_2 domain and 512 or 256 in the t_1 domain. An additional NOESY experiment was performed to identify slowly exchanging amide hydrogen resonances on a freshly prepared D_2O solution after lyophilization of an H_2O sample. For ^{15}N-labeled monellin, 2D ^{1}H−^{15}N HSQC (*31*, *32*), 2D HMQC-J (*33*), 3D NOESY-HSQC (*34*) with mixing times of 50−200 ms, and 3D HOHAHA-HMQC (*35*) with a spin lock time of 78 ms, experiments were performed. Waltz16 was used for ^{15}N decoupling during the acquisition period in all ^{15}N-edited experiments. Slowly exchanging amide protons with solvent water were readily identified from a series of ^{1}H−^{15}N HSQC spectra on a freshly prepared D_2O solution after lyophilization of an H_2O sample for 48 h.

All NMR data were processed using nmrPipe/nmrDraw (Biosym/Molecular Simulations, Inc.) or XWIN−NMR (Bruker Instruments) software on a SGI Indigo^2 workstation. Prior to Fourier transformation in the t_1 dimension, the first row was half-weighted to suppress t_1 ridges (*36*). The DQF-COSY data were processed to 8192 × 1024 data matrixes to obtain a maximum digital resolution for coupling constant measurements. The proton chemical shifts were referenced with internal sodium 4,4-dimethyl-4-silapentane-1-sulfonate (DSS).

Simulated Annealing Calculations and Experimental Constraints. Structure calculations were performed for SCM using a hybrid distance geometry and dynamical simulated annealing protocol with the X-PLOR 3.1 program (Biosym/Molecular Simulations, Inc.) on the SGI Indigo^2 workstation. The modeling protocol was based on the methods implemented previously by Clore and Gronenborn (*37*, *38*) with a small modification by Lee et al. (*39*). The target function for molecular dynamics and energy minimization consisted of covalent structure, van der Waals repulsion, NOE, and torsion angle constraints. The backbone torsion angle and NOE constraints were represented by square-well potentials. On the basis of cross-peak intensities in the NOESY spectra with mixing times of 50−200 ms, the distance constraints were classified as strong (1.8−2.7 Å), medium (1.8−3.3 Å), and weak (1.8−5.0 Å). Pseudoatom corrections were used for methylene protons, methyl groups, and the ring protons of tyrosine residue. For structure generations, a total of 993 inter-residue distance constraints and 56 backbone torsion angle restraints were used during simulated annealing calculations. Among these distance constraints, 319 were intraresidue, 254 were sequential ($|i - j| = 1$), 118 were short-range ($1 < |i - j| \leq 5$), and 206 were long-range ($|i - j| > 5$) NOEs.

Ninety-six hydrogen bond distance constraints were also used by defining two constraints for each bond: $r_{N(i)-O(j)} <$ 3.3 Å and $r_{NH(i)-O(j)} <$ 2.3 Å. A total of 56 torsional angle

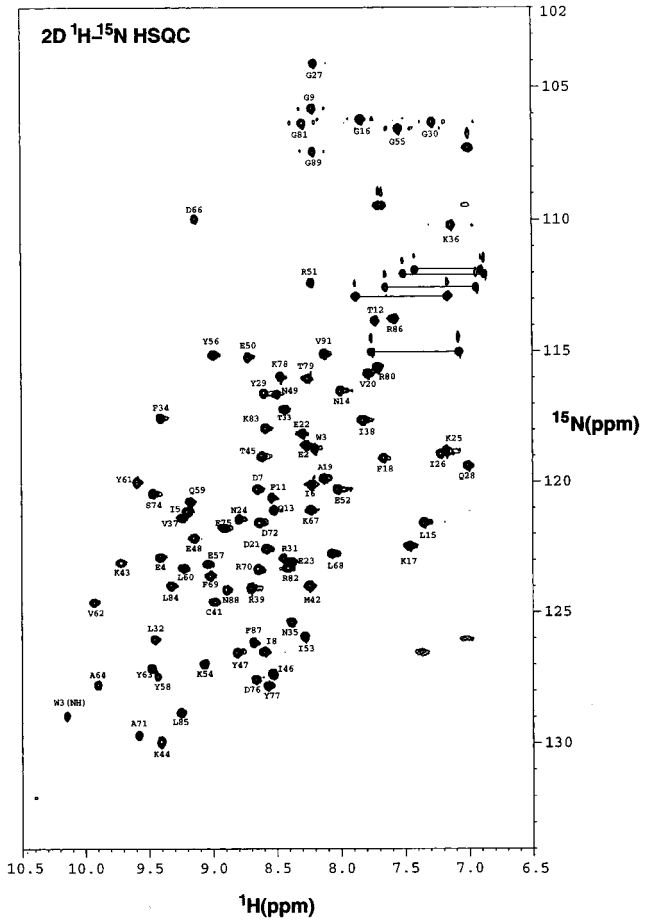

FIGURE 1: Two-dimensional ^{1}H−^{15}N HSQC spectrum of uniformly ^{15}N-labeled SCM with assignments. Cross-peaks connected by dotted lines correspond to Gln and Asn side chain NH_2 groups. The indole NH cross-peak from Trp3 is marked as W3(NH).

constraints were deduced on the basis of the $^3J_{HN\alpha}$ coupling constants from both DQF-COSY and HMQC-J spectra in H_2O solution. For $^3J_{HN\alpha}$ values of >8 Hz, ϕ was constrained to $-120 \pm 50°$; for $^3J_{HN\alpha}$ values of <6.5 Hz, ϕ was constrained to $-55 \pm 45°$ during simulated annealing calculations.

RESULTS AND DISCUSSION

Sequential Resonance Assignments. Spin system assignments were easily made with correlated cross-peaks on homonuclear 2D TOCSY and ^{1}H−^{15}N 3D TOCSY-HSQC spectra. Threonine, leucine, alanine, and valine residues were easily identified by their characteristic methyl proton resonances in the TOCSY spectrum. Glycines were also assigned by their distinctive fingerprint pattern in both 2D DQF-COSY and ^{1}H−^{15}N 2D HSQC spectra (Figure 1). Each of these residues served as a starting point of the sequential resonance assignment procedure. Sequence-specific resonance assignments were completed by following $d_{\alpha N}(i,i+1)$ NOE connectivities starting from NH−C$^\alpha$H cross-peaks of known amino acids (*40*). The side chain proton resonances for all residues were assigned with both ^{1}H−^{15}N 3D TOCSY-HSQC and homonuclear 2D TOCSY connectivities. The observed sequential NOE connectivities for SCM are summarized in Figure 2.

Secondary Structural Elements. Residues from Phe11 to Ile26 formed a stable α-helix. This observation is based on continuous stretches of $d_{NN}(i,i+1)$, $d_{\alpha N}(i,i+3)$, and $d_{\alpha\beta}(i,i+3)$ contacts, small coupling constants ($^3J_{HN\alpha}$), and slowly exchanging amide hydrogens as well as C$^\alpha$H chemical shift indices (Figure 2). On the basis of amide hydrogen exchange data, 34 amide hydrogens were observed to be protected from solvent, which are also involved in secondary structures. A string of intense sequential d_{NN} NOEs for the α-helical region and a continuous stretch of $d_{\alpha N}(i,i+1)$ NOEs for the β-strand were observed from ^{15}N-edited 3D NOESY-HSQC spectra with a mixing time of 150 ms.

An antiparallel β-sheet formed by strands composed of residues 2−5, 36−38, 41−47, 54−64, 69−75, and 83−88 was deduced from both characteristic strong sequential $d_{\alpha N}(i,i+1)$ NOEs and large vicinal $^3J_{HN\alpha}$ coupling constants (>8 Hz) (Figure 2). The antiparallel sheet was defined by backbone−backbone NOEs, and the β-strands were further confirmed by hydrogen bond networks derived from amide hydrogen exchange experiments as well as C$^\alpha$H chemical shift indices (Figure 2). Even though strand β1 was characterized by interstrand NOEs, the amide hydrogens for this region exhibited no slow exchanges with solvent water compared to those of the rest of the strands. Strands β2 and β3 are slightly twisted by a bulge deduced from a $d_{\alpha N}(i,i+3)$ NOE between two strands composed of residues Ile38−Cys41. Three β-turns were identified between β3 and β4, β4 and β5, and β5 and β6, linking two antiparallel strands. Figure 4 summarizes all interresidue NOE contacts for SCM. The chemical shift indices for C$^\alpha$H protons were also calculated from chemical shift differences between observed and random coil values of Wishart et al. (*41*). The computed CSI values agreed well with experimental data as shown in Figure 2.

Three-Dimensional Structures. A total of 50 substructures generated from a distance geometry algorithm were used as starting structures in the simulated annealing stage. Figure 5 shows the number of experimental constraints per residue for SCM. After simulated annealing calculations of 50 starting distance geometry structures, 20 structures ($\langle SA\rangle_k$) showed no constraint violations greater than 0.5 Å for distances and 5° for torsional angles. These structures served for further detailed structural analysis. In Table 1, we list the energies and structural statistics of the final 20 simulated annealing structures related to experimental constraints. The energies and rms deviations of the final structures are within acceptable ranges. The final $\langle SA\rangle_k$ structures converged well with a root-mean-square deviation of 0.96 Å for all backbone atoms, 0.70 Å for backbone atoms except for two loop regions (48−53 and 76−82), and 0.49 Å for residues involved in secondary structures. The restraint energy-minimized (REM) average structure ($\langle\overline{SA}\rangle_{kr}$) from 20 final structures was generated following a restrained energy minimization procedure. This average REM structure exhibited a root-mean-square deviation of 1.19 Å for backbone atoms with respect to 20 $\langle SA\rangle_k$ structures and 0.85 Å for backbone atoms excluding two loop regions (48−53 and 76−82). The deviations from idealized geometry are also very small and satisfy ideal geometry. The $\langle\overline{SA}\rangle_{kr}$ structure clearly displayed the relative orientations between its major secondary structures. The twisted sheet partially wrapped around the beginning of the α-helix. Particularly, the side chains in the bend region of strand β4 have close contacts with those of the α-helix. A best-fit backbone superposition

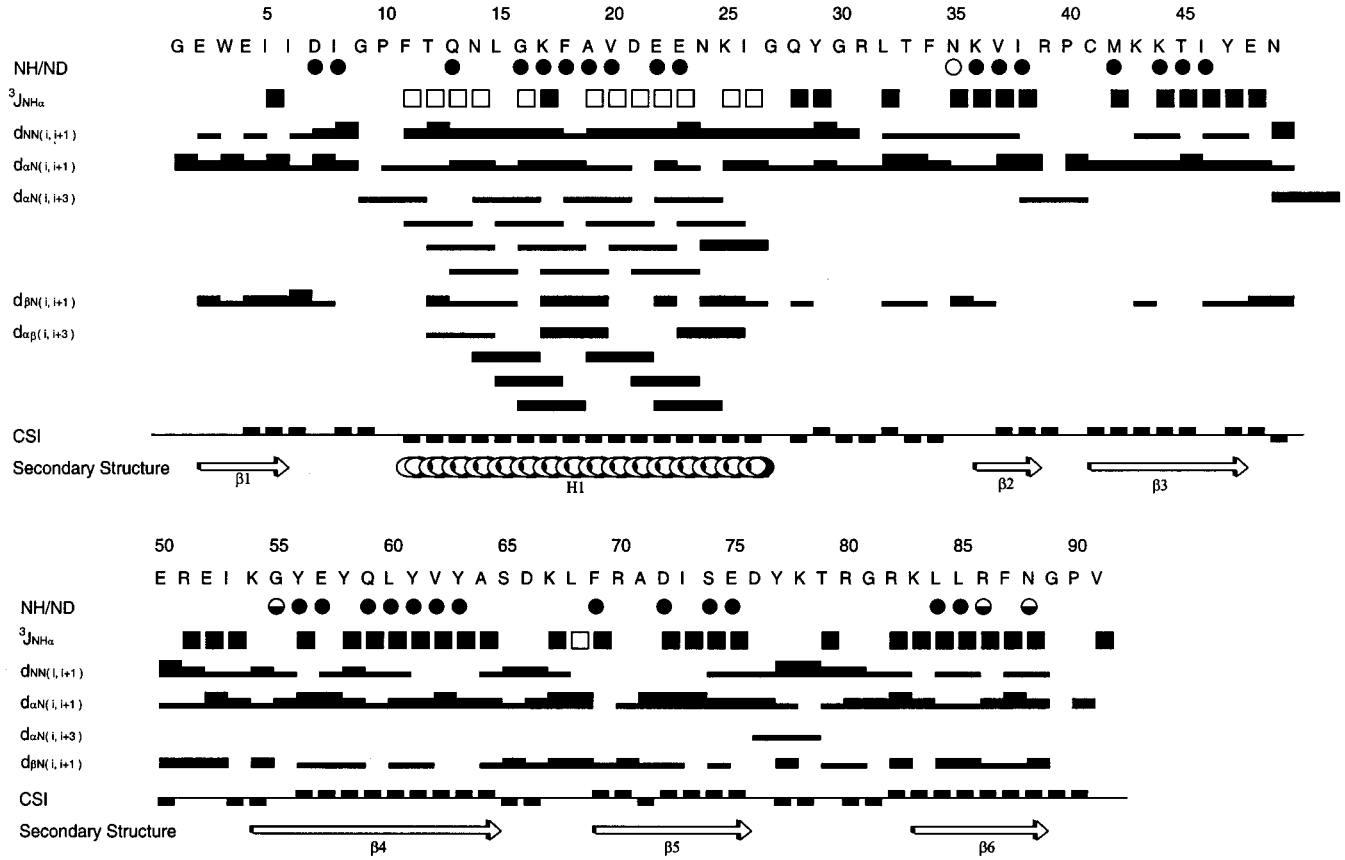

FIGURE 2: Summary of NMR data for the SCM showing the sequential and short-range NOE contacts. Amide proton exchange rates [amide protons survived for 15 (●), 10 (◒), and 5 h (○)], backbone vicinal coupling constants ($^3J_{HN\alpha}$), and chemical shift indices (CSI) calculated for C$^\alpha$H protons are also indicated.

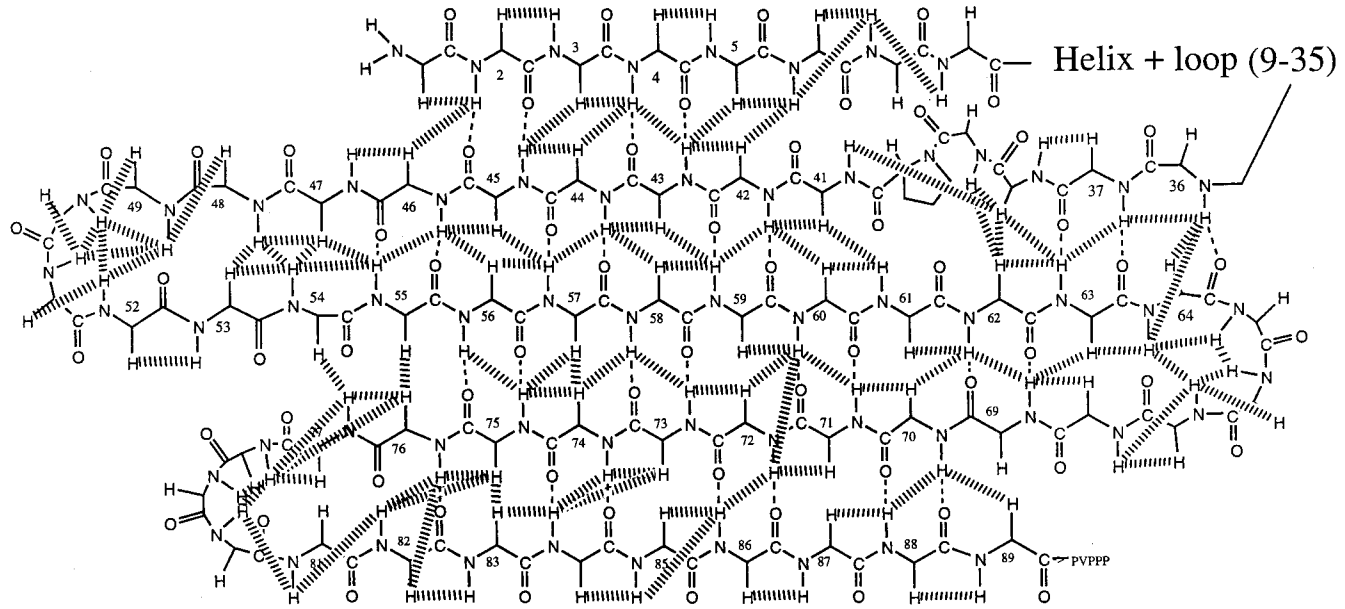

FIGURE 3: Diagram of antiparallel β-sheet regions in SCM. Inter-residue, sequential NOEs as well as hydrogen bonds are shown.

of all final $\langle SA \rangle_k$ structures with average REM structure is displayed in Figure 6. In Table 2, we summarize the statistics associated with the 20 final $\langle SA \rangle_k$ structures of SCM. The atomic average root-mean-square deviations of the final structures are shown in Figure 7A,B. The angular order parameter (*42*) for ϕ and ψ which indicates the degree of dihedral heterogeneity of structures is displayed in Figure 7C. The ϕ and ψ values of most residues except prolines (residues 10, 40, and 90) and loop regions (residues 30−33 and 8) are close to 1, suggesting well-defined backbone angles in the SCM structures. The backbone torsion angles (ϕ and ψ) for 20 $\langle SA \rangle_k$ structures indicate that all of the ϕ and ψ values are distributed in energetically acceptable regions (Figure 8). A MOLSCRIPT representation of the REM average structure shows the general topology of this molecule consists of a long α-helix and a six-stranded

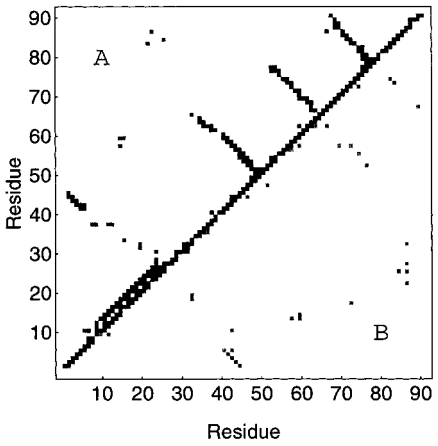

FIGURE 4: Inter-residue NOE contacts for SCM. (A) Backbone−backbone (black boxes) and side chain−side chain (gray boxes) and (B) backbone−side chain NOEs were displayed.

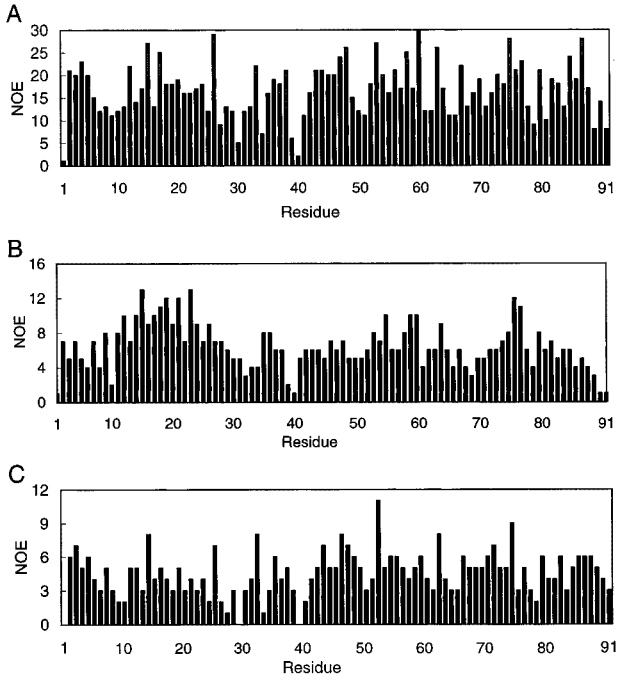

FIGURE 5: Histogram displaying the total number of experimental constraints per residue for SCM. The total number of (A) NOEs, (B) backbone−backbone NOEs, and (C) backbone−side chain NOEs are shown.

antiparallel β-sheet (Figure 9). The main secondary structural elements of SCM are a single 15-residue α-helix formed by residues 11−26 and an antiparallel six-stranded β-sheet spanning residues 2−5, 36−38, 41−47, 54−64, 69−75, and 83−88. Six loops, including an engineered one, were also characterized. It has been proposed that residues Tyr63 in β4 and Asp66 in loop E are common to all sweet peptides, corresponding to the Phe and Asp residues of aspartame. The side chain orientations of Tyr63 and Asp66 have been observed on the side opposite the H1 helix, and those are mostly exposed to solvent.

Figure 10 displays a best-fit superposition of the REM average solution structure over the X-ray crystal structure of SCM. The overall three-dimensional structure of SCM in solution is close to that of X-ray structure. The secondary structural regions which include both the α-helix and six-stranded antiparallel β-sheet are in good agreement. However, the high variability between X-ray and solution structure was observed around the engineered loop D. Differences between the two structures are apparent in the segments of residues 48−53, 65−68, and 27−30, as shown in Figure 10. Particularly, the X-ray crystal structure reported the largest temperature factor for residues 48−53 which comprise loop D. Large rmsd values are also calculated for loop D in the solution structure (Figure 6).

Although both native monellin and SCM were observed as dimers in the crystalline state, SCM is found to exist as a monomer in aqueous solution on the basis of NMR and gel filtration experiments. Since we could not rule out a

Table 1: Structural Statistics for the 20 Final Simulated Annealing Structures of Single-Chain Monellin

parameter	$\langle SA \rangle_k$	$\langle \overline{SA} \rangle_{kr}$
rms deviations from experimental distance restraints (Å)		
all (993)	0.047 (0.039−0.050)[b]	0.038
sequential ($\|i-j\|=1$) (254)	0.049	0.045
short-range ($1<\|i-j\|\le 5$) (118)	0.050	0.045
long-range ($\|i-j\|>5$) (206)	0.047	0.038
intraresidue (319)	0.065	0.064
hydrogen bond (96)	0.031	0.027
rms deviations from experimental dihedral restraints		
dihedral restraints (deg) (56)	0.455 (0.175−0.887)	0.221
energies		
E_{NOE} (all) (kcal mol^{-1})	88.24 (64.76−105.89)	61.13
E_{repel} (kcal mol^{-1})	33.57 (28.96−43.75)	12.06
E_{cdih} (kcal mol^{-1})	1.058 (0.245−1.788)	0.178
E_{L-J} (kcal mol^{-1})[a]	−140.89	−160.90
deviations from idealized covalent geometry		
bonds (Å)	0.031 (0.029−0.034)	0.032
angles (deg)	0.643 (0.621−0.702)	0.645
impropers (deg)	0.515 (0.476−0.569)	0.481

[a] E_{L-J} is the Lennard-Jones/van der Waals potential calculated using the CHARMm empirical energy function. [b] The numbers in parentheses represent minimum and maximum values.

FIGURE 6: Stereoview of the backbone superposition of the energy-minimized average structure ($\langle \overline{SA} \rangle_{kr}$, thick line) over the family of 20 final simulated annealing structures ($\langle SA \rangle_k$, thin line).

Table 2: Atomic rms Deviations for the Final Simulated Annealing Structures of Single-Chain Monellin (91 Residues)

parameters	backbone atoms (Å)	all atoms (Å)
$\langle SA \rangle_k$ vs $\langle \overline{SA} \rangle_k$	0.96 (0.70)[a]	1.69 (1.37)
$\langle \overline{SA} \rangle_{kr}$ vs $\langle \overline{SA} \rangle_k$	0.73 (0.51)	1.11 (0.89)
$\langle SA \rangle_k$ vs $\langle \overline{SA} \rangle_{kr}$	1.19 (0.85)	1.92 (1.64)

[a] rms deviations were calculated for residues excluding two flexible loop regions (residues 48−53 and 76−82).

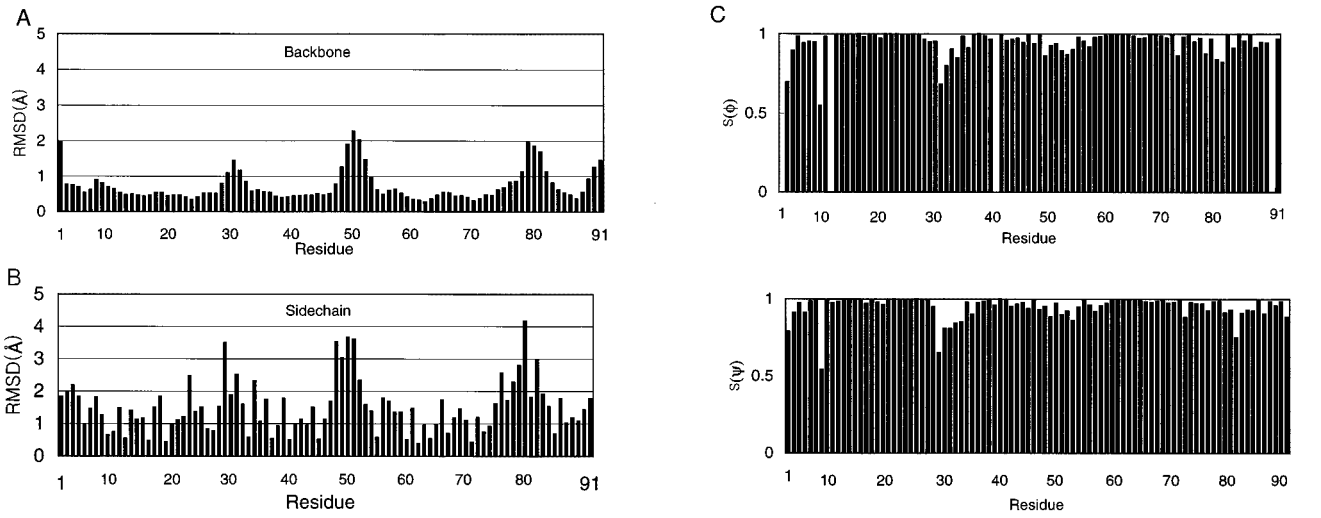

FIGURE 7: Distribution of the average atomic root-mean-square deviations with respect to average structure of the backbone (A) and side chain (B) atoms in the 20 final simulated annealing structures for SCM. Angular order parameters (C) for the backbone and side chains are also displayed.

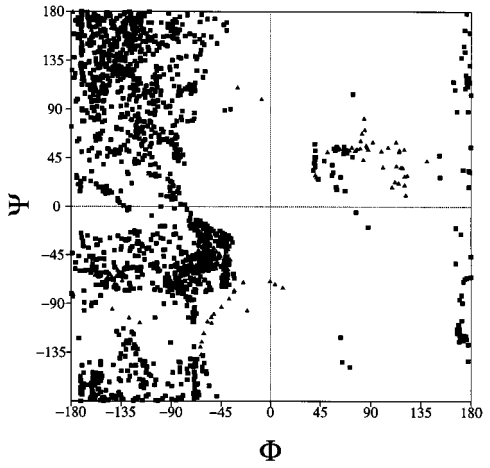

FIGURE 8: Distribution of all ϕ and ψ values for the final simulated annealing structures (20 $\langle SA \rangle_k$) of SCM. The glycine residues are represented by open circles.

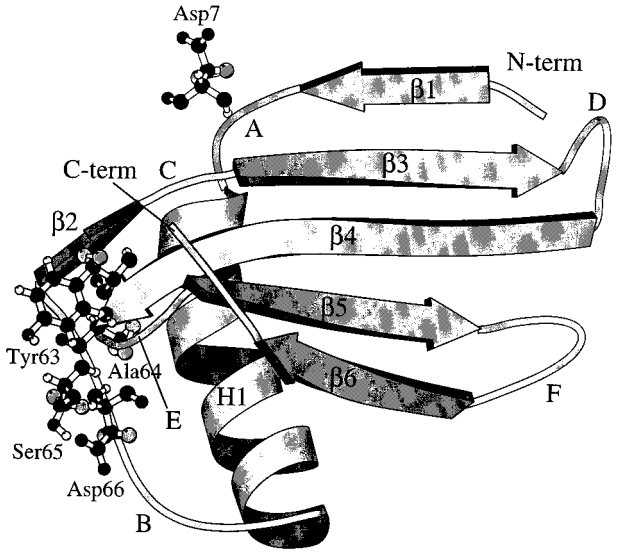

FIGURE 9: Ribbon diagram of the REM average structure displaying ordered secondary structure elements and relative orientation of secondary structures. The side chain atoms for residues responsible for sweetness and receptor binding are also displayed. The figure was generated with MOLSCRIPT (*43*).

possibility that monellin may form a dimer at different salt concentrations, we have performed a series of one-dimensional proton NMR experiments with various salt concentrations (0−500 mM). We found no detectable changes in line width, which implies that salt concentration does not affect monomer and/or dimer formation. The proposed dimeric interface in previous X-ray studies was mainly composed of the hydrophobic amino acids, Trp3, Ile5, Pro40, Met42, Tyr61, and C-terminal prolines. Most of these residues in the solution structure are observed to be solvent-exposed and demonstrated high degrees of flexibility except Met42. Therefore, it is not clear that the dimeric structure is necessary for either sweet taste or receptor binding because it is suggested that SCM exists as a monomer in solution. Unfortunately, both the binding and the mode of interaction of monellin to the sweet receptor molecule are still not well-known.

It has been reported that Arg70 and Arg86 have a close correlation with the degree of sweetness of monellin. Several reports have also indicated that a sulfhydryl group of Cys41 in the beginning of β3 is also critical for sweet taste. In our solution structure, the side chains of cysteine residues are located at the hydrophobic interface between the sheet and the helix. We observed that the side chain of Cys41 maintains the close contact between a bulge comprising residues Ile38−Cys41 and helix H1. It has been suggested that hydrophobic and/or side chain−side chain interactions related to the tertiary structure of monellin are important for sweetness, as well. A recent NMR study of the nonsweet analogue of native monellin has suggested that the side chain of Asp7 is important for sweet taste (*44*). Our solution structure clearly supports this hypothesis, showing all these residues reside on the same surface of the protein (Figure 9). Our solution structure shows that helix H1 has a small bend in the middle, which is similar to that of thiol proteinase inhibitor. In addition, we suppose that the orientation of helix H1 is responsible for the general topology of SCM. Particularly, since most amino acids involved in the biological activity are found in the loop regions, we could conclude that the flexibilities of the side chains are important for both sweet taste and sweet receptor binding.

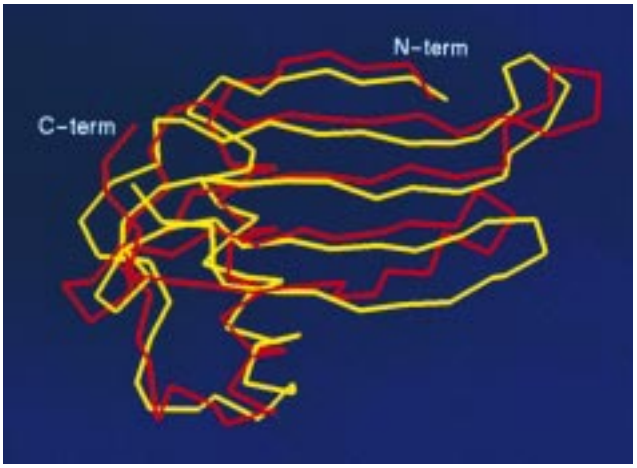

FIGURE 10: Comparison of the backbone conformation for the NMR (yellow) and crystal (red) structures of SCM.

ACKNOWLEDGMENT

The authors thank TMSI Korea for the use of the molecular simulation programs (Molecular Modeling Tools, Molecular Simulations, Inc.). We also thank Dr. Dan Garrett of NIH for providing the programs PIPP and CAPP.

REFERENCES

1. van der Wel, H. (1976) *Biochemistry of Sensory Functions 197*, 235−242.
2. Morris, J. A., and Cagan, R. H. (1972) *Biochim. Biophys. Acta 261*, 114−122.
3. Cagan, R. H. (1984) *Experientia 40*, 843−844.
4. Kohmura, M., Nio, N., and Ariyoshi, Y. (1991) *Agric. Biol. Chem. 55*, 1831−1838.
5. Kohmura, M., Nio, N., and Ariyoshi, Y. (1992) *Biosci. Biotechnol. Biochem. 561*, 472−476.
6. Tancredi, T., Iijima, H., Saviano, G., Amodeo, P., and Temussi, P. A. (1992) *FEBS Lett. 310*, 27−30.
7. Kohmura, M., Nio, N., and Ariyoshi, Y. (1992) *Biosci. Biotechnol. Biochem. 56*, 1937−1942.
8. Somoza, J. R., Cho, J. M., and Kim, S. H. (1995) *Chem. Senses 20*, 61−68.
9. Tonosaki, K., Miwa, K., and Kanemura, F. (1997) *Brain Res. 48*, 234−236.
10. Hellekant, G., Glaser, D., Brouwer, J. N., and van der Wel, H. (1976) *Acta Physiol. Scand. 97*, 241−250.
11. Morris, J. A. (1976) *Lloydia 39*, 25−38.
12. Kurihara, K., and Beidler, L. M. (1968) *Science 161*, 1241−1243.
13. Liu, X., Maeda, S., Hu, Z., Aiuchi, T., Nakaya, K., and Kurihara, Y. (1993) *Eur. J. Biochem. 211*, 281−287.
14. van der Wel, H., and Loeve, K. (1972) *Eur. J. Biochem. 31*, 221−225.
15. Yamashita, H., Theerasilp, S., Aiuchi, T., Nakaya, K., Nakamura, Y., and Kurihara, Y. (1990) *J. Biol. Chem. 265*, 15770−15775.
16. Brouwer, J. N., Hellekant, G., Kasahara, Y., van der Wel, H., and Zotterman, Y. (1973) *Acta Physiol. Scand. 89*, 550−557.
17. Hough, C. A. M., and Edwardson, J. A. (1978) *Nature 271*, 381−383.
18. Ogata, C., Hatada, M., Tomlinson, G., Shin, W. C., and Kim, S. H. (1987) *Nature 328*, 739−742.
19. Fan, P., Bracken, C., and Baum, J. (1993) *Biochemistry 32*, 1573−1582.
20. Murzin, A. Z. (1993) *J. Mol. Biol. 230*, 689−694.
21. Kim, S. H., Kang, C. H., Kim, R., Cho, J. M., Lee, Y. B., and Lee, T. K. (1989) *Protein Eng. 2*, 571−575.
22. Somoza, J. R., Fan, J., Tong, L., Kang, C. H., Cho, J. M., and Kim, S. H. (1993) *J. Mol. Biol. 234*, 390−404.
23. Tomic, M. T., Somoza, J. R., Wemmer, D. E., Park, Y. W., Cho, J. M., and Kim, S. H. (1992) *J. Biomol. NMR 2*, 557−572.
24. Van Geet, A. L. (1970) *Anal. Chem. 42*, 679.
25. Piotto, M., Saudek, V., and Sklenar, V. (1992) *J. Biomol. NMR 2*, 661−665.
26. Lomize, A. L., Sobol', A. G., and Arsen'ev, A. S. (1990) *Bioorg. Khim. 16*, 179−201.
27. Suri, A. K., and Levy, R. M. (1995) *J. Magn. Reson. 106*, 24−31.
28. Bax, A., and Davis, D. G. (1985) *J. Magn. Reson. 65*, 355−360.
29. Rance, M., Soerensen, O. W., Bodehausen, G., Wagner, G., Ernest, R. R., and Wuthrich, K. (1983) *Biochem. Biophys. Res. Commun. 117*, 479−485.
30. Wuthrich, K., Billeter, M., and Braun, W. (1983) *J. Mol. Biol. 169*, 949−961.
31. Bodenhausen, G., and Ruben, D. J. (1980) *Chem. Phys. Lett. 69*, 185−189.
32. Kay, L. E., Keifer, P., and Saainen, T. (1992) *J. Am. Chem. Soc. 114*, 10663−10665.
33. Kay, L. E., and Bax, A. (1990) *J. Magn. Reson. 86*, 110−126.
34. Marion, D., Kay, L. E., Sparks, S. W., Torchia, D. A., and Bax, A. (1989) *J. Am. Chem. Soc. 111*, 1515−1517.
35. Marion, D., Driscoll, P. C., Kay, L. E., Wingfield, P. T., Bax, A., Gronenborn, A. M., and Clore, G. M. (1989) *Biochemistry 28*, 6150−6156.
36. Otting, G., Widmer, H., Wagner, G., and Wuthrich, K. (1988) *J. Magn. Reson. 66*, 187−193.
37. Nilges, M., Clore, G. M., and Gronenborn, A. M. (1988) *FEBS Lett. 229*, 317−324.
38. Nilges, M., Clore, G. M., and Gronenborn, A. M. (1988) *FEBS Lett. 239*, 129−136.
39. Lee, W., Moore, C. H., Watt, D. D., and Krishna, N. R. (1994) *Eur. J. Biochem. 218*, 89−95.
40. Wuthrich, K. (1986) *NMR of Proteins and Nucleic Acids*, John Wiley & Sons, New York.
41. Wishart, D. S., Bigam, C. G., Holm, A., Hodges, R. S., and Sykes, B. D. (1995) *J. Biomol. NMR 5*, 67−81.
42. Hyberts, S. G., Goldberg, M. S., Havel, T. F., and Wagner, G. (1992) *Protein Sci. 1*, 736−751.
43. Kraulis, P. J. (1991) *J. Appl. Crystallogr. 24*, 946−950.
44. Mizukoshi, T., Kohmura, M., Suzuki, E., and Ariyoshi, Y. (1997) *FEBS Lett. 413*, 409−416.

BI9822731